PCCP

ROYAL SOCIETY OF CHEMISTRY

PAPER

Published on 30 July 2026
Licence and permissions

Check for updates

Cite this: *Phys. Chem. Chem. Phys.*, 2026, **28**, 19582

Direct measurement of the temperature dependent lattice and electronic structure reconfigurations of α-$RuCl_3$ thin films

Peixuan Ji,†[a] Jin Chen,†[a] Jiapeng Wang,[a] Liangpeng Hou,[a] Huihui Liang,[a] Jiaying Duan,[a] Xiaochen Hong,[bc] Xi Chen,[d] Zhixin Hu,[d] Bernd Büchner,[b] Xiaosong Wu,[e] Yanqing Ma,[af] Zhixiang Sun*[d] and Lei Ma*[af]

Received 31st January 2026,
Accepted 16th July 2026

DOI: 10.1039/d6cp00368k

rsc.li/pccp

Herein, we reveal the temperature-dependent broadening of the Mott gap in layered α-$RuCl_3$, together with a distinct transition in the range of 100–130 K, through surface morphology and electronic structure characterizations using scanning tunneling microscopy and scanning tunneling spectroscopy, respectively. Furthermore, layer-dependent measurements indicate an enhanced phase transition and Kitaev interactions with decreasing thickness. These results show that low-dimensional α-$RuCl_3$ films differ from their bulk state owing to their unique structural and electronic properties, providing an ideal model platform for exploring Kitaev physics.

Introduction

Quantum spin liquids (QSLs) maintain long range quantum entanglement even at zero temperature due to quantum fluctuations.[1–3] Exploring these exotic quantum states could provide valuable insights for advancing research on high temperature superconductors and topological quantum computation.[4,5] However, fully unveiling and systematically investigating the properties of QSLs remain challenging. Theoretical studies suggest that the Kitaev model, consisting of $S = 1/2$ spins on a honeycomb lattice, offers a fully solvable description of the QSL ground state in 2D systems.[6–8] The anisotropic spin pair interactions along different bonds of the honeycomb lattice compete with one another, resulting in strong frustration and a spin liquid ground state.[3,9]

Recently, d orbital materials have emerged as promising candidates for realizing Kitaev QSLs due to their spatial anisotropy and strong spin orbit coupling.[3,10–13] However, experiments have shown that these QSL candidate materials still retain magnetic order at low temperatures, which hinders further exploration of the intrinsic properties of QSL states.[14–16] Hence, several approaches have been developed to suppress magnetic order, such as the application of high magnetic fields to quench antiferromagnetic order.[1,17–19] Moreover, in addition to applying high magnetic fields, reducing the dimensionality of d orbital materials can also effectively facilitate QSL states, since the large fluctuation effects in low dimensional materials are capable of breaking long range order.[20–22] Additionally, in 2D atomic crystals, magnetic frustration can be substantially amplified, thereby leading to more robust QSL states.[23] Therefore, investigating the physical properties of QSL candidate materials in the low dimensional state represents a promising avenue for deepening our understanding of the Kitaev QSL mechanism.

α-$RuCl_3$ has emerged as a compelling candidate for realizing the Kitaev QSL due to its prominent spin orbit coupling (SOC) effect and electronic correlations arising from the crystal field.[12,24,25] It is an insulating 4d transition-metal halide with honeycomb structured layers composed of nearly ideal edge-sharing octahedra,[24,26] where magnetic moments arise from the Ru^{3+} ($4d^5$) ions located at the centers of $RuCl_6$ octahedra.[9] Intriguingly, its crystal structure resembles that of the 2D magnet CrI_3,[27,28] in which individual atomic layers are stacked together through interlayer van der Waals interactions. The weak interlayer coupling enables the realization of few layer α-$RuCl_3$ materials through mechanical exfoliation, making it an ideal system for studies of the 2D Kitaev model.

The Kitaev QSL in α-$RuCl_3$ has been found to be stable under interlayer coupling, indicating that the 2D α-$RuCl_3$ system may host a topological QSL state.[29] This has triggered a surge of

[a] *Tianjin International Center for Nanoparticles and Nanosystems, Tianjin University, Tianjin, 300072, P.R. China*
[b] *IFW-Dresden, 01069 Dresden, Germany*
[c] *Fakultät für Mathematik und Naturwissenschaften, Bergische Universität Wuppertal, 42097 Wuppertal, Germany*
[d] *Center for Joint Quantum Studies & Department of Physics, School of Science, Tianjin University, Tianjin, 300072, P.R. China. E-mail: zsun@tju.edu.cn*
[e] *School of Physics, Peking University, Beijing, 100871, P.R. China*
[f] *Tianjin Key laboratory for Low-dimensional Electronic Materials and Advanced Instrumentation, Tianjin, 300072, P.R. China*
† Peixuan Ji and Jin Chen contributed equally to this work.

research aimed at elucidating the properties of α-$RuCl_3$ in the low dimensional regime in the past few years. The observed deviations in magnetic scattering in 2D α-$RuCl_3$, compared with its bulk state, indicate a significant enhancement of frustrated magnetic interactions in the 2D system.[23,30] Moreover, as thin α-$RuCl_3$ approaches the 2D limit, the anisotropy of the Kitaev exchange constant increases, indicating the crucial role of crystal structure in the approximate ground state of the QSL.[17] Additionally, electrical transport experiments revealed a gradual increase in resistivity with decreasing temperature and a distinctive transition at around 180 K. Moreover, the structural transition temperature of thin layer α-$RuCl_3$ is higher than that of its bulk counterpart, which can be attributed to the emergence of fractional excitations driven by Kitaev interactions.[31] A recent study of the atomic surface structure and electronic orbital occupancy of monolayer α-$RuCl_3$ grown on highly oriented pyrolytic graphite (HOPG) confirmed its Mott insulating nature, with a band gap of approximately 0.6 eV,[32] and an unconventional Mott transition was observed in few layer α-$RuCl_3$.[33] The latest theoretical results suggest that Majorana zero energy modes (MZMs) in QSLs can be probed through their tunneling conductivity using scanning tunneling spectroscopy (STS).[34] Furthermore, interesting low energy excitations have been observed in monolayer α-$RuCl_3$ tunneling experiments, showing that single layer α-$RuCl_3$ has stronger Kitaev interactions than its bulk counterpart.[35]

However, despite these advances, a systematic understanding of how the atomic structure and local electronic states evolve with thickness, particularly in relation to temperature-driven phase transitions, remains lacking. In particular, direct experimental evidence at the atomic scale linking thickness-dependent structural variation to changes in phase transition temperature has not been established.

To gain deeper insights into 2D QSL properties and the correlation between crystal and electronic structures, we conducted a systematic investigation using temperature-dependent scanning tunneling microscopy (STM) and STS measurements of α-$RuCl_3$ with different thickness. In addition, density functional theory (DFT) calculations were conducted, primarily focusing on geometrical optimization and structural modelling, to assist in the interpretation of the STM/STS results, particularly for atomic-scale configuration identification. The results unveiled a bulk like honeycomb structure and band gap $\approx$ 0.2 eV of the surface layer at 180 K. Differing from the linear temperature dependence of bandgap, thin layered α-$RuCl_3$ show abrupt transition at 100–130 K when the thickness is equal or less 70 nm and accompanying with noticeable degree of configuration distortion.

Experimental

The α-$RuCl_3$ crystals were grown with chemical vapor transport reaction.[36] The layered α-$RuCl_3$ was prepared by mechanical exfoliation from a bulk α-$RuCl_3$ and directly transferred to a STM sample holder in a glove box (MIKROUNA, Ar atmosphere). The thickness of the α-$RuCl_3$ flakes was measured by atomic force microscopy (AFM, Park NX10) in non-contact mode, through the step height differences between the flake and the substrate. The vertical resolution is approximately 0.1 nm, corresponding to an atomic step precision. Then, the sample holder was quickly loaded into STM chamber (RHK PanScan Freedom) to avoid excess air contamination and followed by an annealing treatment ($\sim$150 °C, 1–2 h.) under pressure of 1×10^{-10} Torr. The STM topographies were acquired with a mechanically sheared Pt/Ir alloy tip and calibrated by topographic scanning and dI/dV measurements on an epigraphene film grown on 4H-SiC(0001) surface with a standard lock-in technique.[37] The STS measurements were conducted at temperature ranging from T = 80–180 K. To ensure reproducibility, STM/STS measurements were repeated by approximately fifteen independently prepared flakes and multiple surface regions, yielding consistent results.

DFT calculations were conducted using the Vienna *ab initio* simulation package (VASP). The exchange–correlation energy was calculated using the Perdew–Burke–Ernzerhof functional,[38] combined with the DFT-D3 dispersion correction.[39] The plane wave basis set was used with the projector augmented-wave method to describe the wave function.[40] The energy cutoff for the plane-wave basis set was set to 400 eV, achieving energy convergence of 1 meV per atom. The few-layer $RuCl_3$ was simulated with a 2-layer model and $\sqrt{3} \times \sqrt{3}$ $R30^\circ$ supercell, which contains 12 Ru atoms and 36 Cl atoms. Lattice parameters a and b were optimized to 10.23 Å. All atoms were fully relaxed until the residual force was less than 0.01 eV Å^{-1} for each atom. Vacuum space of 25 Å was added on the out-of-plane direction to avoid periodic interaction. The core-level shift with final-state approximation was introduced to get the correct Fermi level. An electron was removed from the 1s state of each Ru atom and added to the valence orbital. The STM simulation was conducted under the Tersoff–Hamann approximation.

Results and discussion

Surface topography of the bulk α-$RuCl_3$ crystal at 180 K

The crystal structure of bulk α-$RuCl_3$ is shown in Fig. 1(a). Edge sharing $RuCl_6$ octahedra form a honeycomb lattice in the ab plane, and the Ru–Cl layers are stacked along the c direction to form a P3112 structure.[26,28] The Cl–Ru–Cl angles are all within 1° of 90°, and the variation in Ru–Cl bond lengths is within 0.3%, forming a nearly perfect octahedral structure.[24] As shown in Fig. 1(b) and (c), the surface structure of bulk α-$RuCl_3$ was imaged by STM at 180 K, revealing a six-membered ring lattice, which is further verified by the 2D fast Fourier transform of the STM image shown in the inset of Fig. 1(c).

By comparison with theoretically simulated STM images based on DFT calculations, which mainly focus on geometrical modeling, the bright rings can be attributed to six Ru atoms (blue spheres in Fig. 1(d)), while the dark regions correspond to Cl atoms (green spheres in Fig. 1(d)). This is consistent with the projected density of states (PDOS) extracted from the dI/dV

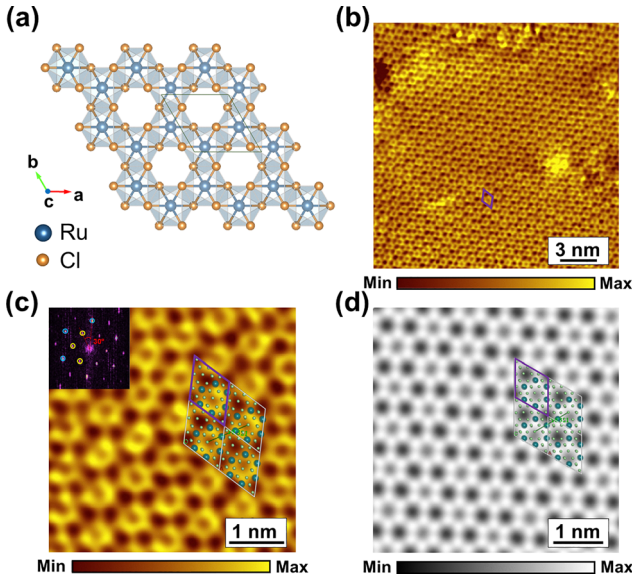

Fig. 1 (a) Schematic depiction of the crystal structure of α-$RuCl_3$ showing edge-sharing $RuCl_6$ octahedra. (b) Constant-current STM topography image of the $RuCl_3$ surface. Setpoint: V_{sample} = −1.12 V, $I_{setpoint}$ = 150 pA. (c) is a closeup view of figure. (b). The purple rhombus in (c) schematically denotes the effective unit cell. Inset: 2D fast Fourier transform of the topography image. (d) Theoretically simulated STM images at V_{sample} = −1.12 V. Blue sphere: Ru atoms; green sphere: Cl atoms.

measurements (SI, Fig. S1), indicating that the bright spots in the STM image correspond to Ru atoms, since Ru atoms have a higher charge density than Cl atoms. Moreover, the STM image also shows a Kekulé bond order with broken symmetry, similar to that observed in graphene.[41,42] The hexagonal honeycomb structure exhibits an enhanced local wave function, as shown in Fig. 1(c) and SI, Fig. S2. This symmetry breaking may facilitate interaction induced phase transitions in the topologically trivial phase,[43] further explaining the influence of crystal structure on the subsequent temperature dependent phase transitions observed in few layer α-$RuCl_3$.

The local density state of bulk α-$RuCl_3$ at 180 K

The local density of states (LDOS) of the α-$RuCl_3$ surface was investigated by STS. The spectrum shows an asymmetric dI/dV particle hole curve with two clearly resolved peaks centered at approximately 0.5 eV and −0.8 eV (Fig. 2(a), red arrows). The appearance of the −0.8 eV peak is consistent with reported angle resolved photoemission spectroscopy (ARPES) results, in which a quasi-flat band located 0.7 eV below the Fermi level was attributed to localized Ru 4d states.[44] As shown Fig. 2(a), a strong suppression of the LDOS is observed between +0.1 eV and −0.1 eV. This indicates the presence of a charge excitation gap around the Fermi level, which is a typical feature of a Mott insulator.[12,45,46] The SOC effect of α-$RuCl_3$ is weaker than that of iridium oxide, but the electron correlation of its 4d orbitals leads to energy band splitting, which further manifests Mott insulator behavior (inset in Fig. 2(a)).[47] Using the band gap fitting method in STM/STS studies,[48,49] a gap of 0.2 eV is established for bulk α-$RuCl_3$ (inset in Fig. 2(b)). This value is

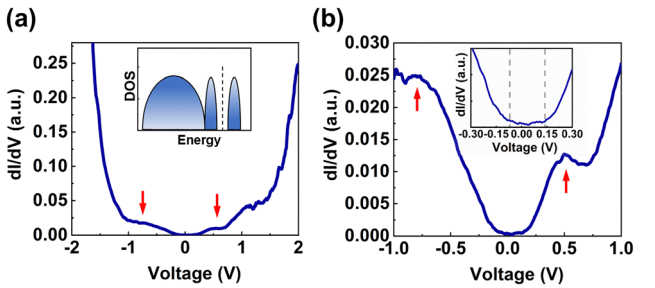

Fig. 2 (a) STS spectra of $RuCl_3$ surface measured at 180 K. Inset: Schematic image of Mott insulator, the electronic states split into a lower and upper Hubbard band separated by the Mott gap. (b) Zoom into the onset region of conduction and valence bands. Setpoint: V_{sample} = 1.0 V, $I_{setpoint}$ = 100 pA.

slightly different from the value of 0.3 eV obtained from X-ray absorption measurements.[24,50] The deviation may be caused by differences in the thickness and temperature of the α-$RuCl_3$ samples used in the two measurements. More details will be discussed in the following paragraphs.

Temperature dependence of electronic properties of bulk sample

Early transport measurements on α-$RuCl_3$, such as temperature-dependent resistance measurements, show an increase in resistance with decreasing temperature. The transition temperature is 150–180 K, which is close to the expected structural transition temperature (from P3112 to $C2/m$) and it is related to Kitaev interaction.[26,51,52] It has been proposed that electron–electron correlations are enhanced due to changes in the crystal structure and affect the electron transition probability,[53] consequently resulting in the temperature dependence of conductivity and a change in slope.[31] To directly investigate the temperature dependence of electron–electron interactions, we measured the electronic properties of bulk α-$RuCl_3$ by variable-temperature STS. To obtain the stable Mott bandgap, the STS experiments were carried out on different tunneling junctions to ensure a constant tunneling gap at each targeting temperature within a rather broad bias range (the detail data are shown in SI, Fig. S3). As shown in Fig. 3(a), the STS results reveal that α-$RuCl_3$ exhibits gaps at all temperatures between 80 and 180 K. To clarify the correlation between the band gap and temperature, the results are presented in Fig. 3(b). The gap clearly decreases with

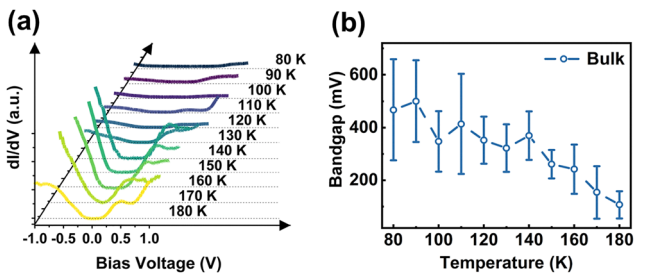

Fig. 3 Temperature-dependent tunneling spectra and bandgap fits of bulk sample. (a) The evolution of the STS spectra measured at temperatures from 80 to 180 K. Setpoint: $I_{setpoint}$ = 150 pA. (b) Temperature dependence of the energy gap determined by the STS spectra.

increasing temperature from 80 to 180 K. Again, this result agrees almost perfectly with the conclusion from traditional transport measurements, as expected for Mott insulators.[31,54,55]

The results further indicate that the interactions between electrons are not solely attributed to changes in the crystal structure, but also to the broadening of the band gap as the temperature decreases, consequently lowering the probability of electron transition. However, no discernible transition point was observed in the band gap temperature dependence experiment conducted on the bulk samples, which instead showed a monotonic linear change. Furthermore, no explicit atomic rearrangements were observed in the surface structure investigation within the temperature range of 80–180 K (see SI, Fig. S4).

Thickness dependent electronic properties of α-$RuCl_3$

To further explore the electronic properties of 2D QSL materials, thickness dependent measurements were conducted, including both STM and STS based temperature dependent band gap investigations. The thicknesses of the mechanically exfoliated α-$RuCl_3$ flakes ranged from 2 to 200 nm. The results reveal that a bandgap transition (the slope of bandgap–temperature curve changes significantly) occurs at temperatures between 100 and 130 K when the thickness is reduced to 70 nm and thinner (Fig. 4(a), SI, Fig. S5 and S6). In line with the established relationship among structure, magnetism, and measured electrical properties, this transition coincides with the emergence of fractionalized excitations in nanoscale flakes due to Kitaev interactions.[31] Furthermore, as the thickness decreases, the transition temperature increases (Fig. 4(b)), which may be attributed to stacking faults introduced during the mechanical exfoliation process.

Defects or changes in crystal structure caused by mechanical exfoliation during sample preparation[56–58] can result in magnetic behaviors distinct from those of bulk materials.[59–61] Surface morphology measurements were conducted on samples with different thicknesses, revealing noticeable lattice distortion as the thickness decreases (SI, Fig. S7), reminiscent of the effect previously reported in exfoliated graphene.[62] Therefore, by using STM, we directly observed the co-occurrence of structural distortions and enhanced phase transitions in α-$RuCl_3$ in the low dimensional regime. Together with the current understanding of dimensionality dependent magnetic interactions[35] and emerging new physical properties,[63] these findings provide insights into the significant correlations among structure, charge, and magnetism in strongly correlated spin systems in low dimensions.

Meanwhile, this result also explains the Raman Spectra observed in the thin α-$RuCl_3$, which exhibits distinctively different characteristics from bulk samples, such as pronounced symmetric forbidden modes and Fano-shaped modes at lower energy levels.[64] This is attributed to the occurrence of structural distortion in materials at low dimensions. Notably, even in a monolayer, the Mott $J_{\mathrm{eff}} = 1/2$ state is still maintained, consistent with the measured scanning tunneling spectroscopy (STS) at a thickness of 2 nm, where it still maintains a Mott bandgap $E_{\mathrm{gap}} \approx 0.6$ eV in 80 K (SI, Fig. S5).

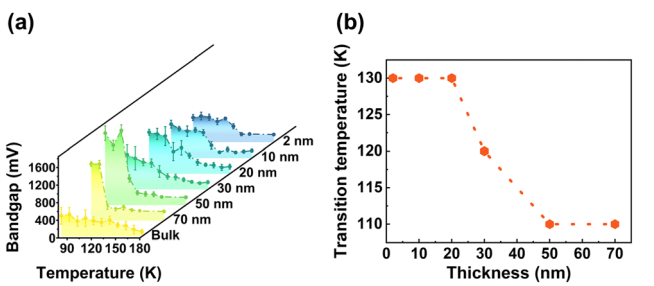

Fig. 4 Temperature *versus* sample thickness diagram of α-$RuCl_3$. (a) Temperature dependence of bandgap as a function of thickness. (b) Thickness dependence of the transition temperature.

Conclusion

In summary, we conducted a thorough and direct investigation of the surface structure and electronic states of α-$RuCl_3$ with various thicknesses at different temperatures through STM and STS measurements. As a potential QSL candidate material, α-$RuCl_3$ demonstrates dimension dependent phase transitions as a function of temperature. Theoretical and experimental observation coincides and verifies that atoms on the surface of bulk α-$RuCl_3$ form an ordered honeycomb structure on the surface and 0.2 eV bandgap at 180 K. An electronic structure transition appears at thickness of 70 nm to 2 nm which is the thinnest sample realized in this work. This suggests that the Kitaev interactions are stronger in thin α-$RuCl_3$ films than in the bulk state. The surface morphology measurements reveal a certain degree of structural distortion as the thickness decreases. This observation is in line with previous predictions of stacking faults occurring due to the mechanical exfoliation process in low dimensions. These results demonstrate the role of dimensionality in the structural and electronic properties, providing more comprehensive insights into the exploration of Kitaev interactions in the 2D limit.

Author contributions

L. M., Z. S., P. J. and J. C. conceived the project. X. H. and B. B. synthesized the bulk α-$RuCl_3$ single crystals. P. J., J. C. and Z. S. performed STM experiment and analysis STM data. J. W., L. H., H. L. and J. D. prepared figures and contributed to the interpretation of the experimental data. X. C. and Z. H. performed DFT calculations. P. J. and J. C. wrote the original draft. L. M., Z. S., X. W. and Y. M. revised and edited the manuscript. all authors participated in the discussions of the results.

Conflicts of interest

There are no conflicts to declare.

Data availability

The availability of data and materials are manuscript and supplementary information (SI). Supplementary information: PDOS, STM image, bias voltage-dependent bandgap, temperature-dependent STM images, tunnelling spectra and energy gap. See DOI: https://doi.org/10.1039/d6cp00368k.

Acknowledgements

This work was financially supported by the National Key R&D Program of China (No. 2022YFC3006303), Tianjin Natural Science Foundation Project (No. 25JCZDJC01380) and the Innovation fund of Haihe Laboratory of Low-dimensional Electronic Materials (25HHDWSS00001 and 25HHDWSS00005).

Notes and references

1 Z. Wang, S. Reschke, D. Huvonen, S. H. Do, K. Y. Choi, M. Gensch, U. Nagel, T. Room and A. Loidl, *Phys. Rev. Lett.*, 2017, **119**, 227202.
2 A. Banerjee, C. A. Bridges, J. Q. Yan, A. A. Aczel, L. Li, M. B. Stone, G. E. Granroth, M. D. Lumsden, Y. Yiu, J. Knolle, S. Bhattacharjee, D. L. Kovrizhin, R. Moessner, D. A. Tennant, D. G. Mandrus and S. E. Nagler, *Nat. Mater.*, 2016, **15**, 733–740.
3 H. Takagi, T. Takayama, G. Jackeli, G. Khaliullin and S. E. Nagler, *Nat. Rev. Phys.*, 2019, **1**, 264–280.
4 C. Nayak, S. H. Simon, A. Stern, M. Freedman and S. Das Sarma, *Rev. Mod. Phys.*, 2008, **80**, 1083–1159.
5 S. D. Sarma, M. Freedman and C. Nayak, *Npj Quantum Inf.*, 2015, **1**, 15001.
6 A. Kitaev, *Ann. Phys.*, 2006, **321**, 2–111.
7 V. M. Katukuri, S. Nishimoto, V. Yushankhai, A. Stoyanova, H. Kandpal, S. Choi, R. Coldea, I. Rousochatzakis, L. Hozoi and J. V. D. Brink, *New J. Phys.*, 2014, **16**, 013056.
8 S. Nishimoto, V. M. Katukuri, V. Yushankhai, H. Stoll, U. K. Rossler, L. Hozoi, I. Rousochatzakis and J. van den Brink, *Nat. Commun.*, 2016, **7**, 10273.
9 M. Majumder, M. Schmidt, H. Rosner, A. A. Tsirlin, H. Yasuoka and M. Baenitz, *Phys. Rev. B*, 2015, **91**, 180401.
10 G. Jackeli and G. Khaliullin, *Phys. Rev. Lett.*, 2009, **102**, 017205.
11 P. H. Chou, C. Y. Mou, C. H. Chung and S. Yip, *npj Quantum Mater.*, 2025, **10**, 90.
12 H. S. Kim, V. Shankar, A. Catuneanu and H. Y. Kee, *Phys. Rev. B*, 2015, **91**, 241110.
13 A. Sahasrabudhe, D. A. S. Kaib, S. Reschke, R. German, T. C. Koethe, J. Buhot, D. Kamenskyi, C. Hickey, P. Becker, V. Tsurkan, A. Loidl, S. H. Do, K. Y. Choi, M. Grüninger, S. M. Winter, Z. Wang, R. Valentí and P. H. M. van Loosdrecht, *Phys. Rev. B*, 2020, **101**, 140410.
14 J. A. Sears, M. Songvilay, K. W. Plumb, J. P. Clancy, Y. Qiu, Y. Zhao, D. Parshall and Y.-J. Kim, *Phys. Rev. B*, 2015, **91**, 144420.
15 X. Liu, T. Berlijn, W. G. Yin, W. Ku, A. Tsvelik, Y. J. Kim, H. Gretarsson, Y. Singh, P. Gegenwart and J. P. Hill, *Phys. Rev. B*, 2011, **83**, 220403.
16 A. H. Abdeldaim, H. Gretarsson, S. J. Day, M. D. Le, G. B. G. Stenning, P. Manuel, R. S. Perry, A. A. Tsirlin, G. J. Nilsen and L. Clark, *Nat. Commun.*, 2024, **15**, 9778.
17 I. A. Leahy, C. A. Pocs, P. E. Siegfried, D. Graf, S. H. Do, K. Y. Choi, B. Normand and M. Lee, *Phys. Rev. Lett.*, 2017, **118**, 187203.
18 S. H. Baek, S. H. Do, K. Y. Choi, Y. S. Kwon, A. U. B. Wolter, S. Nishimoto, J. van den Brink and B. Buchner, *Phys. Rev. Lett.*, 2017, **119**, 037201.
19 J. Zheng, K. Ran, T. Li, J. Wang, P. Wang, B. Liu, Z. X. Liu, B. Normand, J. Wen and W. Yu, *Phys. Rev. Lett.*, 2017, **119**, 227208.
20 K. Kim, S. Y. Lim, J. U. Lee, S. Lee, T. Y. Kim, K. Park, G. S. Jeon, C. H. Park, J. G. Park and H. Cheong, *Nat. Commun.*, 2019, **10**, 345.
21 N. D. Mermin and H. Wagner, *Phys. Rev. Lett.*, 1966, **17**, 1133–1136.
22 D. Lin, K. Ran, H. Zheng, J. Xu, L. Gao, J. Wen, S. L. Yu, J. X. Li and X. Xi, *Phys. Rev. B*, 2020, **101**, 045419.
23 L. Du, Y. Huang, Y. Wang, Q. Wang, R. Yang, J. Tang, M. Liao, D. Shi, Y. Shi, X. Zhou, Q. Zhang and G. Zhang, *2D Mater.*, 2018, **6**, 015014.
24 K. W. Plumb, J. P. Clancy, L. J. Sandilands, V. V. Shankar, Y. F. Hu, K. S. Burch, H. Y. Kee and Y.-J. Kim, *Phys. Rev. B*, 2014, **90**, 041112.
25 A. Banerjee, J. Yan, J. Knolle, C. A. Bridges, M. B. Stone, M. D. Lumsden, D. G. Mandrus, D. A. Tennant, R. Moessner and S. E. Nagler, *Science*, 2017, **356**, 1055–1059.
26 M. Ziatdinov, A. Banerjee, A. Maksov, T. Berlijn, W. Zhou, H. B. Cao, J. Q. Yan, C. A. Bridges, D. G. Mandrus, S. E. Nagler, A. P. Baddorf and S. V. Kalinin, *Nat. Commun.*, 2016, **7**, 13774.
27 L. Zhang and Y. Motome, *Phys. Rev. B*, 2024, **110**, L241109.
28 N. Ubrig, Z. Wang, J. Teyssier, T. Taniguchi, K. Watanabe, E. Giannini, A. F. Morpurgo and M. Gibertini, *2D Mater.*, 2019, **7**, 015007.
29 S. S. Zhang, C. D. Batista and G. B. Halász, *Phys. Rev. B*, 2025, **111**, L161104.
30 T. T. Mai, A. McCreary, P. Lampen-Kelley, N. Butch, J. R. Simpson, J. Q. Yan, S. E. Nagler, D. Mandrus, A. R. H. Walker and R. V. Aguilar, *Phys. Rev. B*, 2019, **100**, 134419.
31 S. Mashhadi, D. Weber, L. M. Schoop, A. Schulz, B. V. Lotsch, M. Burghard and K. Kern, *Nano Lett.*, 2018, **18**, 3203–3208.
32 Z. Wang, L. Liu, H. Zheng, M. Zhao, K. Yang, C. Wang, F. Yang, H. Wu and C. Gao, *Nanoscale*, 2022, **14**, 11745–11749.
33 X. Zheng, K. Jia, J. Ren, C. Yang, X. Wu, Y. Shi, K. Tanigaki and R. R. Du, *Phys. Rev. B*, 2023, **107**, 195107.
34 T. Bauer, L. R. D. Freitas, R. G. Pereira and R. Egger, *Phys. Rev. B*, 2023, **107**, 054432.
35 B. Yang, Y. M. Goh, S. H. Sung, G. Ye, S. Biswas, D. A. S. Kaib, R. Dhakal, S. Yan, C. Li, S. Jiang, F. Chen, H. Lei, R. He, R. Valenti, S. M. Winter, R. Hovden and A. W. Tsen, *Nat. Mater.*, 2023, **22**, 50–57.
36 R. Hentrich, A. U. B. Wolter, X. Zotos, W. Brenig, D. Nowak, A. Isaeva, T. Doert, A. Banerjee, P. Lampen-Kelley,

D. G. Mandrus, S. E. Nagler, J. Sears, Y. J. Kim, B. Buchner and C. Hess, *Phys. Rev. Lett.*, 2018, **120**, 117204.
37 P. Lauffer, K. V. Emtsev, R. Graupner, T. Seyller, L. Ley, S. A. Reshanov and H. B. Weber, *Phys. Rev. B*, 2008, **77**, 155426.
38 J. P. Perdew, K. Burke and M. Ernzerhof, *Phys. Rev. Lett.*, 1996, **77**, 3865–3868.
39 S. Grimme, J. Antony, S. Ehrlich and H. Krieg, *J. Chem. Phys.*, 2010, **132**, 154104.
40 P. E. Blochl, *Phys Rev B Condens Matter*, 1994, **50**, 17953–17979.
41 X. Liu, G. Farahi, C. L. Chiu, Z. Papic, K. Watanabe, T. Taniguchi, M. P. Zaletel and A. Yazdani, *Science*, 2022, **375**, 321–326.
42 A. Coissard, D. Wander, H. Vignaud, A. G. Grushin, C. Repellin, K. Watanabe, T. Taniguchi, F. Gay, C. B. Winkelmann, H. Courtois, H. Sellier and B. Sacepe, *Nature*, 2022, **605**, 51–56.
43 M. Kharitonov, S. Juergens and B. Trauzettel, *Phys. Rev. B*, 2016, **94**, 035146.
44 I. Pollini, *Phys Rev B Condens Matter*, 1996, **53**, 12769–12776.
45 P. Phillips, *Rev. Mod. Phys.*, 2010, **82**, 1719–1742.
46 F. Lüpke, S. Manni, S. C. Erwin, I. I. Mazin, P. Gegenwart and M. Wenderoth, *Phys. Rev. B*, 2015, **91**, 041405.
47 A. Koitzsch, C. Habenicht, E. Müller, M. Knupfer, B. Büchner, H. C. Kandpal, J. van den Brink, D. Nowak, A. Isaeva and T. Doert, *Phys. Rev. Lett.*, 2016, **117**, 126403.
48 A. J. Bradley, M. M. Ugeda, F. H. da Jornada, D. Y. Qiu, W. Ruan, Y. Zhang, S. Wickenburg, A. Riss, J. Lu, S. K. Mo, Z. Hussain, Z. X. Shen, S. G. Louie and M. F. Crommie, *Nano Lett.*, 2015, **15**, 2594–2599.
49 R. M. Feenstra, J. Y. Lee, M. H. Kang, G. Meyer and K. H. Rieder, *Phys. Rev. B*, 2006, **73**, 035310.
50 L. Binotto, I. Pollini and G. Spinolo, *Phys. Status Solidi B*, 1971, **44**, 245–252.
51 A. Glamazda, P. Lemmens, S. H. Do, Y. S. Kwon and K. Y. Choi, *Physical Review B*, 2017, **95**, 174429.
52 H. B. Cao, A. Banerjee, J. Q. Yan, C. A. Bridges, M. D. Lumsden, D. G. Mandrus, D. A. Tennant, B. C. Chakoumakos and S. E. Nagler, *Phys. Rev. B*, 2016, **93**, 134423.
53 N. F. Mott, A Journal of Theoretical Experimental and Applied Physics, *Philos. Mag.*, 2006, **34**, 643–645.
54 N. S. Kini, A. M. Strydom, H. S. Jeevan, C. Geibel and S. Ramakrishnan, *J. Phys.: Condens. Matter*, 2006, **18**, 8205–8216.
55 M. Jenderka, J. Barzola-Quiquia, Z. Zhang, H. Frenzel, M. Grundmann and M. Lorenz, *Phys. Rev. B*, 2013, **88**, 045111.
56 C. H. Lui, Z. Li, Z. Chen, P. V. Klimov, L. E. Brus and T. F. Heinz, *Nano Lett.*, 2011, **11**, 164–169.
57 J. H. Warner, M. H. Rummeli, T. Gemming, B. Buchner and G. A. Briggs, *Nano Lett.*, 2009, **9**, 102–106.
58 M. Velicky, P. S. Toth, A. M. Rakowski, A. P. Rooney, A. Kozikov, C. R. Woods, A. Mishchenko, L. Fumagalli, J. Yin, V. Zolyomi, T. Georgiou, S. J. Haigh, K. S. Novoselov and R. A. Dryfe, *Nat. Commun.*, 2017, **8**, 14410.
59 N. Sivadas, S. Okamoto, X. Xu, C. J. Fennie and D. Xiao, *Nano Lett.*, 2018, **18**, 7658–7664.
60 D. Soriano, C. Cardoso and J. Fernández-Rossier, *Solid State Commun.*, 2019, **299**, 113662.
61 S. W. Jang, M. Y. Jeong, H. Yoon, S. Ryee and M. J. Han, *Phys. Rev. Mater.*, 2019, **3**, 031001.
62 J. S. Bunch, A. M. van der Zande, S. S. Verbridge, I. W. Frank, D. M. Tanenbaum, J. M. Parpia, H. G. Craighead and P. L. McEuen, *Science*, 2007, **315**, 490–493.
63 L. Kong, M. Papaj, H. Kim, Y. Zhang, E. Baum, H. Li, K. Watanabe, T. Taniguchi, G. Gu, P. A. Lee and S. Nadj-Perge, *Nature*, 2025, **640**, 55–61.
64 J. H. Lee, Y. Choi, S. H. Do, B. H. Kim, M. J. Seong and K. Y. Choi, *Npj Quantum Inf.*, 2021, **6**, 43.